Grain Growth Behavior in Electrodeposited Nanocrystalline FeCoNi Medium-entropy Alloy

Atsuya Watanabe[1,*], Takahisa Yamamoto[2], Koichiro Nambu[3] and Yorinobu Takigawa[1]

[1]*Department of Materials Science, Graduate School of Engineering, Osaka Metropolitan University, Sakai 599-8531, Japan*
[2]*Department of Materials Design Innovation Engineering, Graduate School of Engineering, Nagoya University, Nagoya 464-8603, Japan*
[3]*Department of Mechanical Engineering, Graduate School of Engineering, Osaka Sangyo University, Daito 574-8530, Japan*

Bulk nanocrystalline FeCoNi MEA with a high tensile strength was developed recently. Grain refinement is a hopeful approach to achieving excellent mechanical properties in HEAs/MEAs, however, the thermal stability of microstructure in the alloy has not been clarified enough. In this study, we investigated microstructure evolution in nanocrystalline FeCoNi MEA annealing at a 300–1000 °C temperature range. Sharp increases in the grain size were repeatedly found. Each plateau range formed respective orientations.

Keywords: *grain growth, nanocrystal, medium-entropy alloy, thermal stability*

1. Introduction

The electrodeposition process for bulk nanocrystalline FeCoNi medium-entropy alloy (MEA) was developed in 2022 [1)]. High entropy alloys (HEAs) and MEAs are emerging alloy classes with an innovative strategy for design [2, 3)]. These alloys are composed of equiatomic several metal elements. The condensed alloying elements let to form simple phases constitutions, such as a single solid solution, induce lattice distortions, sluggish diffusion, and other synergistic effects. Particularly, stabilizing of solid solutions is implemented from the gain of configuration entropy and contributes to improving ductility avoiding precipitations, which can behave as origins of the fracture. Grain refinement is considered a consistent strengthening approach with the concept of HEAs/MEAs because it can increase strength without adding further elements. In fact, several studies have already demonstrated the high strength of HEAs/MEAs with fine grains or nanocrystals, further, a large Hall-Petch slope compared to conventional alloys [1, 4, 5)].

One of the universal concerns for nanocrystalline materials is the stability of microstructure. It restricts not only fabrication methods but also applied temperature. We could overcome the former via electrodeposition, which is low temperature process. The latter may be solved by slow diffusion rate in some HEAs/MEAs. Some studies fragmentally demonstrated the thermal stability of microstructure in the FeCoNi MEA. Haché et al. [6)] reported a rapid increase after 400 °C for 1 h annealing in electrodeposited nanocrystalline FeCoNi MEAs. On the other hand, Wu et al [7)] and Lavakumar et al. [8)] reported the microstructure evolution in casted FeCoNi MEAs. The former reported the occurrence of abnormal grain growth after annealing at 800 °C for 1 h, whereas it was not found in the latter. The authors pointed out the probability of abnormal grain growth in the previous studies may have been incurred by contamination from the atmosphere during annealing. Regardless, the grain growth behavior in FeCoNi MEA has not been clarified in a wide temperature range enough. In this study, we investigated the grain growth behavior of FeCoNi MEA during annealing to clarify a potential applied temperature range of it.

2. Experiment

2.1 Alloy preparation

Nanocrystalline equiatomic FeCoNi MEA was prepared on a copper substrate by electrodeposition. A 5-L aqueous solution for the electrodeposition was composed by 600-mol m^{-3} boric acid, 50-mol m^{-3} hydroxylammonium chloride, 15-mol m^{-3} saccharin sodium dihydrate, 5.0-mol m^{-3} sodium dodecyl sulfate, 500-mol m^{-3} nickel(II) sulfamate tetrahydrate, 80-mol m^{-3} cobalt(II) sulfate heptahydrate, and 220-mol m^{-3} iron(II) sulfate heptahydrate. These chemicals were supplied by FUJIFILM Wako Pure Chemical (Japan). For anodes, two platinized titanium rods were employed. During the electrodeposition, solution temperature was maintained at 55 ± 4 °C. Details of electrodeposition were described elsewhere [1)]. The composition uniformity of the deposited alloy was confirmed by energy-dispersive X-ray spectroscopy using a Quantax XFlash 6-10 detector (Bruker, USA) on an SU8010 scanning electron microscope (SEM; Hitachi High-Tech, Japan) at a 15-kV acceleration voltage. The atomic composition of the alloy was determined as $Fe_{34.3}Co_{31.1}Ni_{34.6}$.

2.2 Characterization of grain growth behavior

The obtained alloy was cut out in several tips. These tips were annealed in a muffle furnace with an air atmosphere at 300–1000 °C for 1 h and quenched in water. The copper substrate was mechanically ground off prior to the annealing using silicon carbide paper. For microstructure analysis, the surface of the tips was ground using SiC paper and buff polished with 1-μm diamond powder, and finished by buff polishing with colloidal silica.

To observe microstructure in the annealed tips, orientation imaging microscopy (OIM) was performed using an MSC-2200 detector (TSL Solutions, Japan) attached to a JSM-7001F SEM (JEOL, Japan) at 15-kV acceleration voltage. X-ray diffraction measurement was also performed using Ultima IV system (Rigaku, Japan) at a 40-kV acceleration voltage.

* Graduate Student, Osaka Metropolitan University

3. Results and discussion

Inverse pole figure (IPF) maps which consisted of collected OIM data in the annealed alloys are shown in Fig. 1. It indicates the microstructure evolution during annealing at each temperature for 1 h. Regarding the as-deposited alloy and the alloys annealed at 300 °C, any diffraction pattern was not detected. This fact suggests that the grain size in these alloys is comparable to or smaller than the spatial resolution of the SEM. In the alloys which were annealed at 400–800 °C (Figs. 1a–e), major grains are indicated in blue, i.e., they are orientated <111> direction. On the other hand, many grains indicated in green or red also appeared in the alloys that are annealed at 900 and 1000 °C (Figs. 1f and 1g). In these two alloys, some cracks are also observed along grain boundaries. Previous studies in electrodeposited nickel alloys reported that embrittlement can be caused by a condensation of particular impurities on grain boundaries during grain growth [9]. The segregation of sulfur in particular, which exists in the solution for electrodeposition as additive agents and metal salts, is regarded as a causal impurity of significant embrittlement. The finding of cracks in the alloys which were annealed at 900 °C or higher implies the occurrence of thermal embrittlement also in electrodeposited MEAs with a similar mechanism.

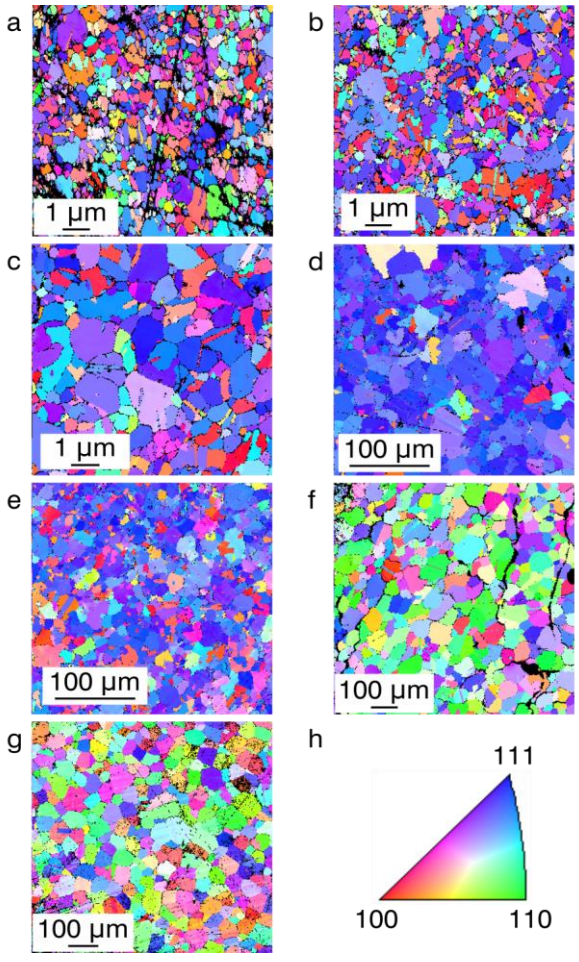

Figure 1 IPF maps of FeCoNi MEA annealed at (a) 400, (b) 500, (c) 600, (d) 700, (e) 800, (f) 900, and (g) 1000 °C for 1 h. (h) Color legend.

XRD profiles of these alloys are shown in Fig. 2. Here, these profiles can be classified in four types: (a) wide diffraction peaks, (b) 111 and 200 diffraction peaks and a constant proportion of their intensity, (c) only strong 111 diffraction peak, and (d) several diffraction peaks including 220. At first, wide diffraction peaks were detected in profiles of the as-deposited alloy and the alloy annealed at 300 °C. Generally, grain refinement below micron increases the width of the diffraction peaks. The crystallite size of the as-deposited alloy and the alloy annealed at 300 °C were 8 and 10 nm, respectively, in estimation from the 111 diffraction peaks via

$$d = K\lambda / B\cos\theta \quad (1)$$

where, λ is the X-ray wavelength, B is the full width at half maximum the intensity of the peak, and θ is the Bragg angle [10]. For the shape factor, K, 0.9 was applied. Second, as suggested in OIM analysis, the strong <111> preferred orientation was composed in the alloys which were annealed at 400 °C or higher temperature. However, it is notable that the intensity proportion of a strong 111 diffraction and a weak 200 diffraction were constant in the alloys which were annealed between 400 and 600 °C, and 200 diffractions were not detected barely in the samples which were annealed at 700 and 800 °C, contrastively. Finally, in the alloys which were annealed at 900 and 1000 °C, 220 diffractions were also clearly detected. At this stage, it is believed that the microstructure in the alloy recrystallized fully and composed a random orientation.

The grain size evolution in the alloy was summarized in Fig. 3 The representative values for grain size were computed from OIM data. The error bars for grain size indicate standard deviations. Crystallite sizes were

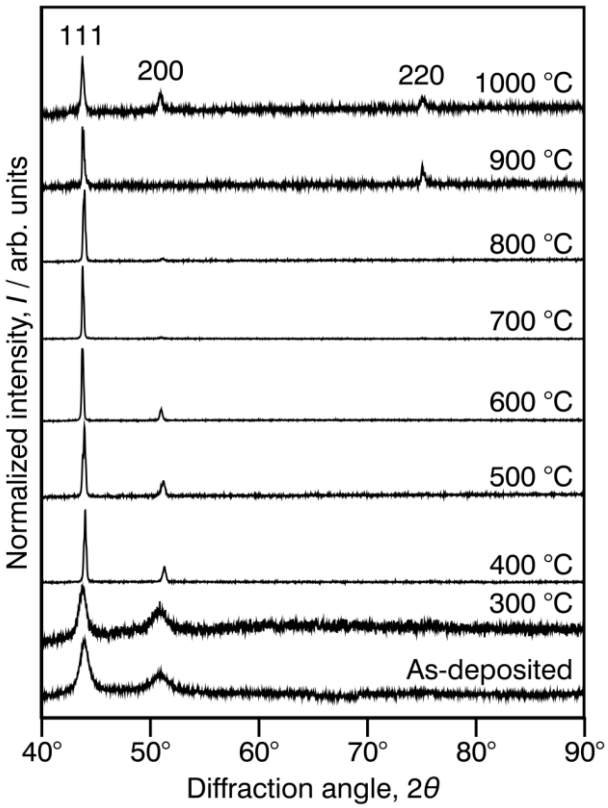

Figure 2 XRD profiles as-deposited and annealed alloys.

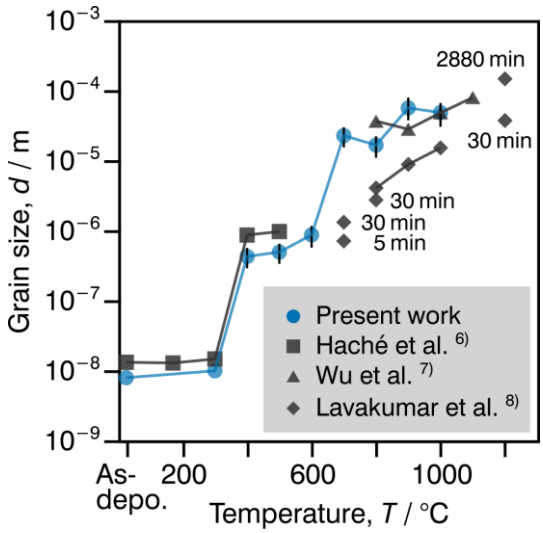

Figure 3 Grain size evolution post annealing at several temperatures in present work and the literature [6–8].

employed for the grain sizes in the as-deposited alloy and the alloy annealed at 300 °C. Regarding the annealing below 300 °C, grain growth occurred hardly, and the grain size of the alloy was stable. The first sharp rise in grain is found at 400 °C. Although higher temperature annealing brings on larger grain sizes, the difference in sizes post-annealing was slight between 400–600 °C. Annealing at 700 °C led the grain size to jump again, and the size finally exceeded 10 μm. Then, the grain size seems to suddenly increase again at 900 °C. This increment was 3.4 times, though it is smaller than spikes found at other temperatures. Further, the grain size slightly decreased from 700 to 800 °C and from 900 to 1000 °C. Although the mechanism of abnormal grain growth has not been unveiled enough, the driving force for it is reduction of grain boundary energy. The frequency of abnormal grain growth can be described as

$$N = A \exp(-Q/RT) \quad (2)$$

where Q is the apparent activation energy, R is the gas constant, T is the absolute temperature. Thus, these two small decreases in grain size are explained by an increase in the number of grains that can grow and competition between them [11].

Abnormal grain growth has been found also in some conventional alloys, whereas it is intriguing that the grain size repeatedly spikes in the present alloy. It should be emphasized that these spikes in grain size correspond to the boundaries between types of XRD profiles. The fact that abnormal grain growth formed respective orientations in each stage implies that different modes of grain growth activated in each temperature. It is not easy to clarify the origin of it, nevertheless, segregation of alloying elements to specific sites [12, 13] may affect it.

4. Summary

Grain growth behavior in nanocrystalline FeCoNi MEA was investigated over the 300–1000 °C temperature range. The grain size in the present alloy rapidly increased at multiple temperatures. Each temperature stage of annealing also formed respective orientation.

Acknowledgments

This work was supported by the Japan Society for the Promotion of Science KAKENHI Grant Numbers JP22K04778 and JP23KJ1828. Elemental analysis was performed using the SEM at Equipment Sharing Center for Advanced Research and Innovation, Osaka Metropolitan University.

References

1) A. Watanabe, T. Yamamoto and Y. Takigawa: Sci. Rep. **12** (2022) 12076.
2) J.W. Yeh, S.K. Chen, S.J. Lin, J.Y. Gan, T.S. Chin, T.T. Shun, C.H. Tsau and S.Y. Chang: Adv. Eng. Mater. **6** (2004), 299–303.
3) B. Cantor, I.T.H. Chang, P. Knight and A.J.B. Vincent: Mater. Sci. Eng. A. **375–377** (2004) 213–218.
4) S. Yoshida, T. Ikeuchi, T. Bhattaharjee, Y. Bai, A. Shibata and N. Tsuji: Acta Mater. **171** (2019) 201–215.
5) A. Watanabe, T. Yamamoto, R. Miyamoto and Y. Takigawa: Mater. Sci. Technol. (in print) doi: 10.1080/02670836.2023.2187973.
6) M.J.R. Haché, T. Jason, U. Erb and Y. Zou: J. Alloys Compd. (2022) 163233.
7) Z. Wu, H. Bei, F. Otto, G.M. Pharr and E.P. George: Intermetallics **46** (2014) 131–140.
8) A. Lavakumar, S. Yoshida, J. Punyafu, S. Ihara, Y. Chong, H. Saito, N. Tsuji and M. Murayama: Scr. Mater. **230** (2023) 115392.
9) A. Watanabe and Y. Takigawa: Results Surf. Interfaces. **1** (2020) 100001.
10) P. Scherrer: Nachr. Ges. Wiss. Göttingen, Math.-Phys. Kl. (1918) 98–100.
11) I. Matsui, A. Watanabe, T. Uesugi, N. Omura, Y. Takigawa and T. Yamamoto: Materialia **8** (2019) 100481.
12) K. Shiotani, T. Niiyama and T. Shimokawa: Mater. Trans. **61** (2020) 1272–1279.
13) L. Li, Z. Li, A.K. Silva, Z. Peng, H. Zhao, B. Gault and D. Raabe: Acta Mater. **178** (2019) 1–9.